RESEARCH PAPER

Effects of nickel layer on interfacial micro-structure distribution and macro-mechanical properties for vacuum-brazed dissimilar steel joints

Leilei Wang[1] · Nian Li[1] · Xinlong Wei[2] · Xiang Ling[1] · Qingsheng Li[1]

Abstract

In this paper, nickel-plated Q235 carbon steel and 304 stainless steel were vacuum brazed together using pure copper foil as the filler metal. The effects of nickel plating at the carbon steel surface on the shear strength of the brazed joints were investigated and verified by the finite element analysis method. The microstructure and shear strength of the brazed dissimilar steel joints were characterized by SEM and tensile experiments. The results found that the pure copper brazing material exhibited excellent wettability to the base metal. With the increase of heat treatment temperature and holding time, the plated Ni particles fuse with each other and the boundary of the Ni particles gradually disappears, which increases the diffusion distance of Fe, Ni, and P elements and the width of the interface transition zone. The maximum shear strength of the brazed dissimilar steel joint without the nickel layer is 265.9 MPa for the optimized brazing parameters with 0.06-mm thickness of pure copper foil. After nickel plating on the carbon steel surface with heat treatment of 500 ℃ for 1 h, the shear strength of the brazed dissimilar steel joint reduces to 213.4 MPa, which may be due to the formation of brittle intermetallic compounds by Ni and P elements on the surface of the layer at high temperatures.

1 Introduction

The gas wave refrigerator (GWR) is a frequently employed apparatus within the natural gas sector [1]. Its operational principle involves exploiting the motion of gas within an oscillating tube to effectuate a decrease in gas pressure for the purposes of refrigeration. However, the oscillating tube, which is a critical component of the GWR, presents certain manufacturing challenges, specifically with respect to its hub and blade. Such components are mainly manufactured through integral machining characterized by relatively low efficiency. Furthermore, it is worth noting that the connection between the hub and blade of the oscillating tube is susceptible to failure under external loading in service, potentially leading to degradation in the mechanical capacity of the oscillating tube. Therefore, in order to ensure the safe and reliable operation of the GWR, it is crucial to improve both the manufacturing efficiency of the oscillating tube and the connection strength between its hub and blade.

Brazing is a widely employed joining method in various industries such as aviation and petrochemical equipment, owing to its ability to provide a strong joining between components through the filling of weld seams [2–5]. Excellent wetting and fluidity are particularly utilized between the liquid filler material and the base material at high temperatures. The application of brazing in manufacturing processes holds significant promise, as it can streamline the production process while minimizing the deformation of oscillation tube components. Nevertheless, considering unexpected debonding or fracture of brazing interfaces between the oscillating tube and the blades, the relation of interface microstructures and macro-mechanical behaviors is required

---

✉ Nian Li
linian@njtech.edu.cn

✉ Xiang Ling
xling@njtech.edu.cn

1 School of Mechanical and Power Engineering, Nanjing Tech University, Nanjing 211816, China

2 College of Mechanical Engineering, Yangzhou University, Yangzhou 225127, China

to be characterized to improve structural performance under severe operating conditions.

The selection of appropriate brazing materials for vacuum brazing of stainless steel requires the use of high-temperature brazing materials such as copper-based, nickel-based, silver-based, and iron-based materials [4, 6–8]. Among these, copper-based brazing materials are the most widely used due to their excellent processability, wetting performance, caulking ability, joint strength, and cost-effectiveness in brazing various metals [4, 9–12]. Wang et al. [13] employed an aluminum foil sandwich in induction diffusion brazing and found that the intermetallic compound layer consisted of Cu_9Al_4 and $CuAl_2$ with a thickness of 2 μm. Xiao et al. [14] used Zn-3Al braze in ultrasonic-assisted brazing and found that well-bonded Al/Cu joints could be obtained without the utilization of any brazing flux. Some well-formed welds with a maximum tensile and shear load of 154 N/mm were also achieved via CMT fusion brazing [15]. Jiang YU et al. [16] performed successfully the dissimilar materials joining of C/C composites to T2 copper by thermo-compensated resistance brazing welding with AgCuTi filler powder. A laser brazing process was developed by Solchenbach et al. [17] for dissimilar Al-Cu connections. The process exhibits the formation of homogenous interface structures with a remarkable reduction in intermetallic compound thickness, reaching as low as 3.2 μm. When the thickness of the Al-Cu combination is 210–200 μm, the maximum shear strength reaches 121 MPa.

Coating the surface of the base material can facilitate the materials that are otherwise difficult to weld into ones that are easier to weld, and can modify the microstructure and morphology of the base material, thereby improving the failure strength of the brazed structural joints. Zhao et al. [18] constructed successfully wavy microstructure for enhancing bonding strength in TA2/Q235 brazed joints with Ni and MC-Cr multilayer at 770 °C for 20 min. Choudhary et al. [19] investigated vacuum brazing of stainless steel and copper plates using a silver-based filler alloy, particularly focusing on the effect of electrochemically applied 30-μm-thick nickel coatings on the braze-zone microstructure. Scanning electron microscopy analysis reveals that nickel-coated stainless steel exhibits improved joint integrity and soundness compared to uncoated stainless steel when brazing is performed at 830 °C. However, at a higher brazing temperature of 860 °C, cracks are observed in the copper side of the joint, attributed to the faster diffusion of Cu atoms from the copper plate compared to Ni atoms from the nickel coating. Furthermore, the shear strength of the joints significantly decreases due to the presence of cracks, indicating the importance of achieving crack-free joints for optimal mechanical performance. In a study conducted by Beura et al. [10], the brazing of aluminum bronze and stainless steel was investigated using silver-copper-based brazing media. To improve the wetting characteristics of the brazing material, the researchers incorporated Zn elements into the brazing media, which had the effect of lowering the melting point and increasing the wettability of the brazing material. Additionally, to further improve wetting, a 5-μm-thick pure nickel was plated on both sides of the base material. This technique effectively mitigated the dissolution of aluminum bronze, prevented intermetallic compound growth in the brazing seam, and therefore improved the bonding strength. The influence of Ni in the Ag–Cu filler on the wetting behavior and brazing characteristics of stainless steel was investigated by Mu G et al. [20] through wetting tests and brazing tests conducted under high vacuum conditions. The addition of Ni in the Ag–Cu filler resulted in enhanced wettability of the filler metal and improved joint strength. Zhang et al. [21] employed the magnetron sputtering method to coat a 3-μm-thick nickel layer on tin bronze and martensitic stainless steel. The primary objective was to enhance the wetting performance of the brazing material on the base material, facilitate the generation of copper-based and nickel-based solid solutions at both sides of the interface, and improve the mechanical properties of the interface tissue. As a result, the tensile strength of the joint increased significantly to 260 MPa. Zhang C et al. [22] chose the cold metal transfer (CMT) welding-brazing process to join Al alloy and Ni-coated steel. The results demonstrated that the presence of a nickel coating enhanced the wettability and spreadability of the molten AlSi12 filler metal on the surface of the steel substrate. Kumar et al. [23] conducted a comparative study to investigate the impact of various surface states of the base material on the microstructure and mechanical properties of joints during vacuum brazing with silver-copper eutectic brazing material at 800 °C. The researchers observed that compared to the pickling activation or ultrasonic cleaning of the stainless steel surface, the application of nickel-plated joints on the stainless steel surface led to obvious diffusion of the brazing material along the grain boundaries of the base plate manufactured

Table 1 The chemical composition of base materials (wt.%)

Material	C	P	Si	Mn	Cr	Ni	S	Fe
Q235 mild steel	0.018	0.14	0.21	0.53	-	-	-	Balance
304 stainless steel	0.08	-	0.78	-	18.09	7.80	0.06	Balance

Fig. 1 The schematic diagram of the shear tensile sample
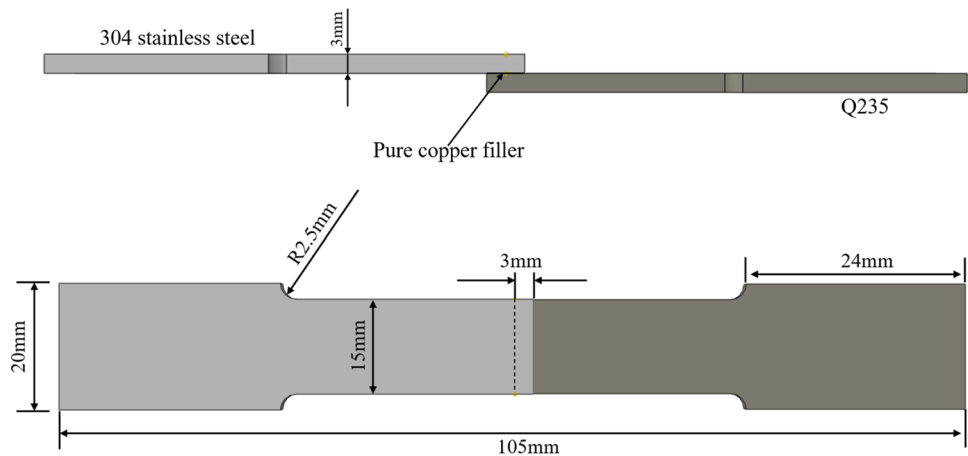
by purple copper. It resulted in substantial intergranular infiltration, which significantly reduced the toughness of the joints. Sanchez et al. [24] studied the effect of stainless steel surface nickel plating thickness on vacuum-brazed joints between stainless steel and bronze. The study showed that the brazed joints with 20–30-µm-thick nickel plating had a multilayer microstructure and high Ni element content due to the thick nickel layer. However, the difference in Ni and Cu interdiffusion rates was too large, resulting in holes at the copper side interface and consequently reducing the mechanical properties of the joints. Conversely, the brazed joints with 3–4-µm-thick nickel plating on the stainless steel surface did not show any obvious microstructural defects and exhibited good mechanical properties. Mu et al. [25] studied the effect of nickel plating on grain boundary penetration during vacuum brazing of copper and 304 stainless steel. They found that the molten filler predominantly infiltrated the Cu substrate through high-angle boundaries. This infiltration along grain boundaries resulted in the formation of stress concentration at the groove.

The present study employed a vacuum brazing technique to join 304 stainless steel and Q235 mild steel by utilizing pure copper filler metal. Since chemical nickel plating presents its inherent advantages in addressing the issue

of mild steel corrosion, the base plates manufactured by Q235 mild steel have been coated with a Ni layer before vacuum brazing. Moreover, heat treatment of the mild steel was conducted after chemical nickel plating, with the aim of improving the bonding strength between the plated layer and the base plate. The properties of the brazed joints without heat treatment, specifically with respect to the macro shear strength, microstructure, and element distribution in the brazing area, were compared with those of mild steel that had undergone nickel plating and subsequent heat treatment. Finally, a micro finite element model (FEM) of representative volume element (RVE) was proposed to characterize the impact of the thickness of the nickel plating layer and the size of the spherical particles on the macro failure strength of the vacuum-brazed joint. The formation of brittle compounds in the brazing process is closely related to the composition of the solder metal, the gap of the brazing joint, the brazing temperature, the holding time, and other factors, which directly affect the interaction process between brazing and the base metal. Therefore, how to obtain the best brazing process parameters is crucial to control the formation of intermetallic compounds in the brazing seam and obtaining a good weld-quality product. There are still shortcomings in the research of this part of this paper, which will be investigated in subsequent work.
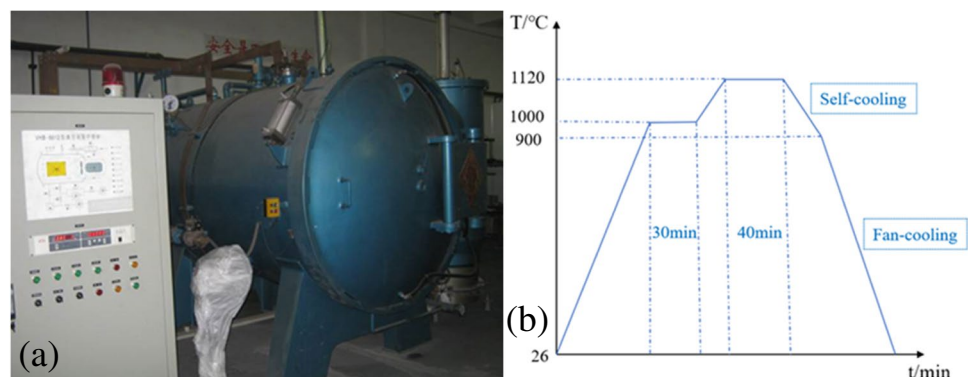
Fig. 2 **a** Vacuum brazing furnace and **b** Brazing process curve

Fig. 3 INSTRON 5869 material testing machine

2 Experimental procedures

2.1 Sample preparation

The present study utilized Q235 mild steel and 304 stainless steel, of which the nominal thickness was 3 mm, as the base metals for investigation. The chemical composition of the base materials is presented in Table 1. The data in Table 1 are provided by two manufacturers. Q235 is from Shenzhen Amanda Hardware Steel Co., Ltd, in China, and 304 stainless steel is from Wuxi Zhuoxu Metal Co., Ltd, in China.

The experiments in this paper are equivalent to being divided into three groups. The first group is directly brazing under different solder thicknesses. The second group and the third group are after nickel plating, one group is brazed after heat treatment, and the other group is directly brazed without heat treatment.

As shown in Fig. 1, the samples were designed to be a bone-shaped plate with a nominal overlapped length of 3 mm, to keep in accordance with GB11363 standard for the strength of brazed joints. Other detailed dimensions are marked in Fig. 1. To investigate the influence of various initial brazing material thicknesses on the quality of brazed joints, three different thicknesses of brazing material, namely 0.03 mm, 0.06 mm, and 0.12 mm, were employed for the brazing process.

Selective plating of nickel exclusively onto the Q235 mild steel prior to vacuum brazing can serve as corrosion protection while also reducing economic costs. Before electroless plating, the Q235 sample was successively polished with 600, 800, and 1500 grits sandpaper, then degreased and cleaned. The surface of the Q235 sample was coated with a Ni layer under the condition of electroless plating at 89 ℃ for 1 h. The composition of the electroless Ni plating solution is listed below: 20 g/L $NiSO_4 \cdot 6H_2O$, 25 ml/L $CH_3CH(OH)COOH$, 26 g/L $NaH_2PO_2 \cdot H_2O$, 14 g/L CH_3COONa, 3 ml/L CH_3CH_2COOH, a small amount of CH_4N_2S, and a suitable amount of $C_{18}H_{29}NaO_3S$.

When applied after nickel plating, before vacuum brazing, heat treatment can boost the bonding strength between the plating and the carbon steel substrate. The Q235 sample coated with Ni layer was heat-treated using a tubular furnace at 400, 500, and 600 ℃ for 1 h or 500 ℃ for 0.5, 1, and 1.5 h. The argon was blown into the furnace for half an hour to exhaust the air before heating and continuously introduced at a flow rate of 0.5 L/min throughout the heat treatment process. The schematic diagram of the shear tensile sample is shown in Fig. 3. The chemical composition of base metals is shown in Table 1.

The lap length and brazing thickness were 3 mm and 0.06 mm, respectively. Prior to welding, the stainless steel underwent polishing to eliminate the oxide film, while the nickel-plated carbon steel specimens underwent a 30-min ultrasonic cleaning with an acetone-ethanol solution.

2.2 Vacuum brazing process

The VHB-6612 vacuum brazing furnace, as shown in Fig. 2a, mainly consisted of a heating system, a vacuum system, a cooling system, and a control system. The vacuum level in the furnace was kept below 0.01 Pa during the

Table 2 The shear strength of different-parameter brazed joints

The thickness of brazing material (mm)	Shear strength (MPa)	Standard deviation	Coefficient of variation (%)
0.03	251.6	21.3	8.5
0.06	265.9	5.10	1.9
0.12	192.7	17.3	9.0

Fig. 4 Microstructure of the brazed joints with different filler metal thicknesses: **a** 0.03 mm, **b** 0.06 mm, and **c** 0.12 mm
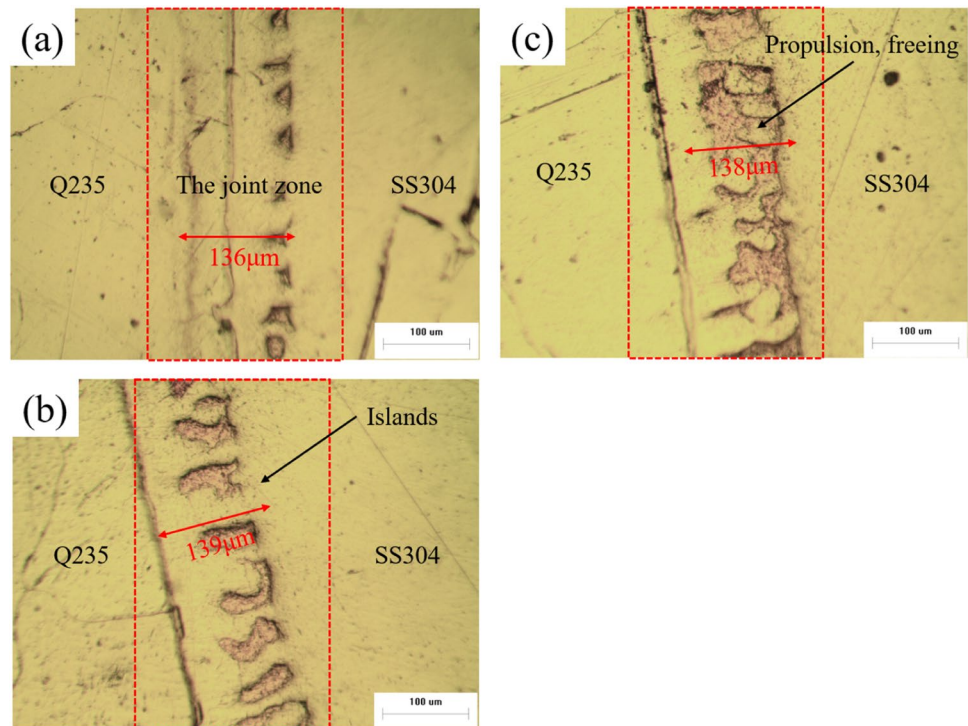
whole brazing process. The detailed brazing process curve is presented in Fig. 2b. During the experiment, regardless of nickel plating or not, heat treatment or not, the same brazing process curve was used.

From Fig. 2b, the whole process is shared, and the detailed explanation is as follows: (1) extraction stage: vacuum degree is about 0.01 Pa. Its purpose is to remove metal surface oxide film and increase surface moisture; (2) heating stage: for small heat stress, slow heating up to 1000 °C; (3) thermal insulation stage: thermal insulation at 1000 °C for 30 min, sufficient heat exhaustion gas during the process; (4) heating stage: continuous slow heating to flame temperature 1120 °C; (5) heat-retaining stage: under the temperature of 1120 °C, keep warm for 40 min to fully disperse the metal elements; (6) vacuum slow cooling: from room temperature up to 1120 °C, use vacuum slow self-cooling, and the purpose is to use at high temperature to apply stress at the beginning of the flame, prevent cracking production, and raise the temperature strength; (7) fast cooling: to prevent non-steel sensitization problem, starting from 900 °C, filling gas in the furnace, simultaneous cooling vacuum furnace fan, using structure rapid cooling to room temperature after furnace.

It is the control of the vacuum, holding time, and other factors in the brazing process that avoids the generation of obvious joint defects.

2.3 Tensile experiment for brazed joints and microscopic characterization

The microstructure of the dissimilar brazed joints was characterized using optical microscopy and scanning electron microscopy with energy-dispersive spectroscopy (SEM, JSM-6360LV). The shear strength of the brazed joints was carried out by INSTRON 5869 material testing machine. Charge placement method, different thickness charges for different parts in different joints, the final tool is installed in the first place. A composition such as upper model, lower model, screw plug, etc. The upper and lower model is a square plate, size 200 mm × 200 mm × 12.5 mm. The upper and lower plates are fixed by screw plugs, and the upper plate is left on the upper plate according to the amount of pressure.

To conduct the tensile test, the test specimen is initially secured to the designated position of the testing machine via a bolt. A slight pre-tension is then applied to the specimen through pre-tensioning operations to ensure proper alignment with the collet. The lap specimen is subsequently clamped as depicted in Fig. 3.

The testing machine is subsequently loaded at a continuous rate of 0.2 mm/min until the specimen sustains damage. The resultant damage load and mode of failure are recorded for subsequent analysis.

Fig. 5 Element distribution result of the brazed joint
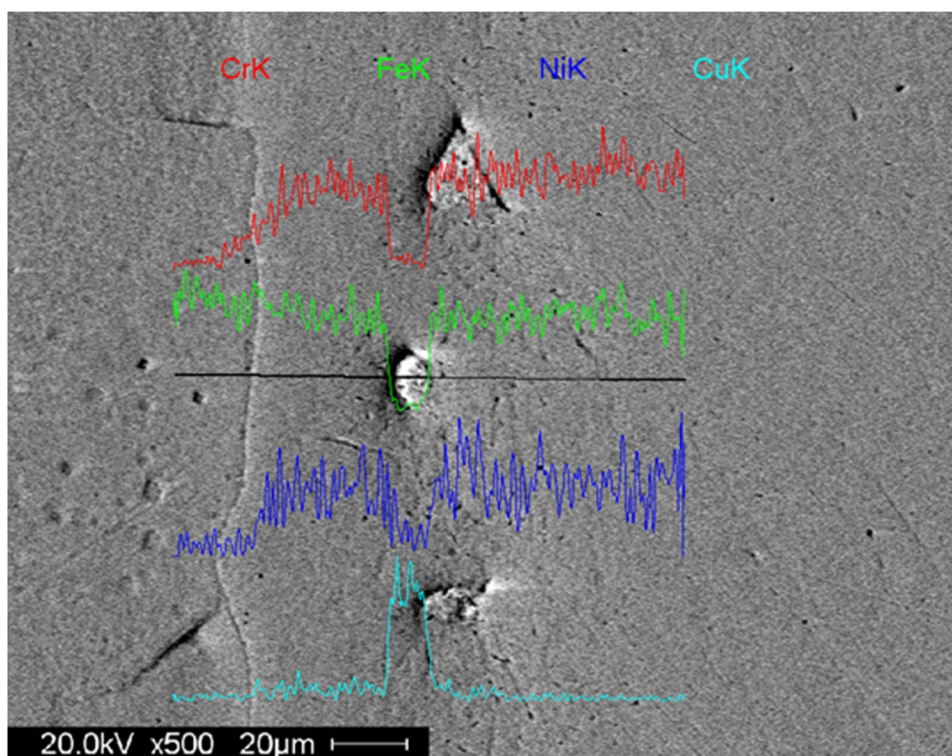
3 Experimental results and analysis

3.1 Analysis of brazed joint without nickel layer

The shear strength of brazed joint without nickel-plater is tested by INSTRON under three kinds of solder thicknesses. At least three brazing samples are taken for each group, and the results are averaged, as shown in Table 2.

The experimental results show that the shear strength of each group of brazed joints is higher than 190 MPa, and the maximum shear strength is as high as 265.9 MPa. The coefficient of variation was within 9%, and the smallest coefficient of variation is only 1.9%. The shear strength increases first and then decreases as the thickness of the

Fig. 6 EDS measurement position of the micro-zone in the brazed joint

brazing material increases. The shear strength of the preset 0.06-mm solder is the largest, and the preset 0.12 mm is the smallest. Because of the preset thinner solder, the gap between the solder joints is small, the capillary action is strong, the molten solder spreads smoothly on the surface of the base metal, the wetting effect is good, and the interaction with the base metal is sufficient, and it is easy to form a dense solder joint. At the same time, the gap between the brazing seam is small, the distance required for elements to diffuse from one end of the base metal to the other end of the base metal becomes smaller, the interaction between the base metal and the brazing material is enhanced, the degree of alloying of the brazing seam structure increases, and the islands in the brazing seam. The proportion increases, and the strength of the joint increases. However, if the solder is too thin, due to the difficulty in ensuring the surface flatness of the base metal and the existence of some defects, it will also lead to insufficient filling and affect the strength of the joint [26].
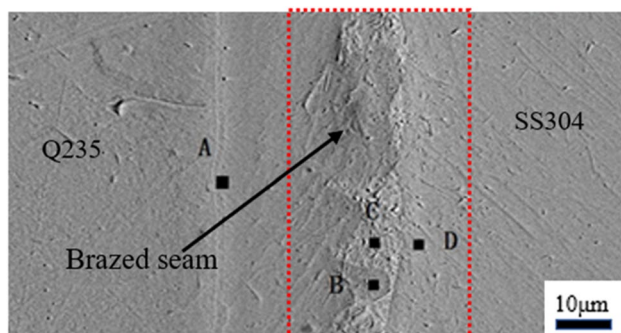
Table 3 EDS results of the micro-zone in the brazed joint (wt/%)

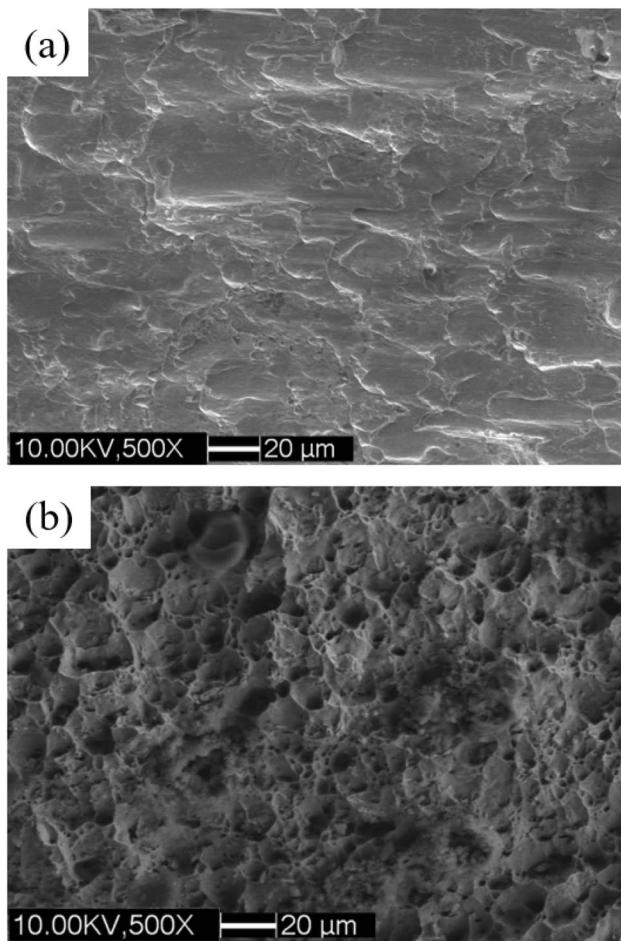| Position	Cr	Fe	Ni	Cu
A	6.87	88.85	0.86	3.42
B	17.12	67.00	7.74	8.14
C	0.94	4.30	2.17	92.59
D	19.25	72.51	8.24	-

Fig. 7 The microcosmic appearances of the fracture of brazed joints: **a** pure copper and **b** Q235

The microstructure of the brazed joints with different filler metal thicknesses is shown in Fig. 4. It can be seen that different thicknesses of pure copper fill the gaps and form a brazed joint consisting of Q235 steel, Q235 steel/copper, copper, copper/304 stainless steel, and 304 stainless steel. The brazed joint with 0.03 mm thickness

of pure copper exhibits a tightly bonded interface with 70-µm width. The brazed joint with 0.06-mm thickness of pure copper forms the 100-µm-thickness brazed seam, in which an island extends from the Q235 carbon steel/copper interface to the pure copper interlayer, connecting the two base metals. The brazed joint with 0.12-mm pure copper is tightly bonded and forms the 130-µm-thickness brazed seam, in which the Q235 carbon steel/copper interface produces islands advancing toward the pure copper intermediate layer and Q235 carbon steel is not fully connected with 304 stainless steel by the islands due to the part of the islands gradually breaking away from Q235 carbon steel interface.

Joint strength is closely related to the width of the brazing seam and the brazing material. Prado et al. [27] obtained high metal continuity in brazed joints with thicker copper layers under brazing conditions of 1135 ℃-10 min and 1100 ℃-10 min. The reduced brazed filler thickness can decrease the brazed seam width and promote the extension of the islands, which in turn connects Q235 carbon steel and 304 stainless steel. In conditions of high load, the liquid brazed filler at high temperature will be squeezed out of the brazed seam, which is not conducive to the penetration of the islands through the brazed filler layer to connect Q235 carbon steel and 304 stainless steel.

The element distribution result of the brazed joint with 0.06-mm-thickness pure copper and 2.64 kg load is shown in Fig. 5. As can be seen from the figure, Fe, Cr, Ni, and Cu elements have diffused and Cr and Ni elements in 304 stainless steel diffuse into the copper intermediate layer with the dissolution of the parent metal. High concentrations of Fe, Cr, and Ni elements are observed in the islands. In the island area, the copper element content has increased significantly, and the copper content that can be seen here has been added to the island's production.

The EDS measurement position and results of the microzone in a brazed joint with 0.06-mm thickness of pure

Fig. 8 Microscopic morphology of Q235 **a** before nickel plating and **b** after nickel plating
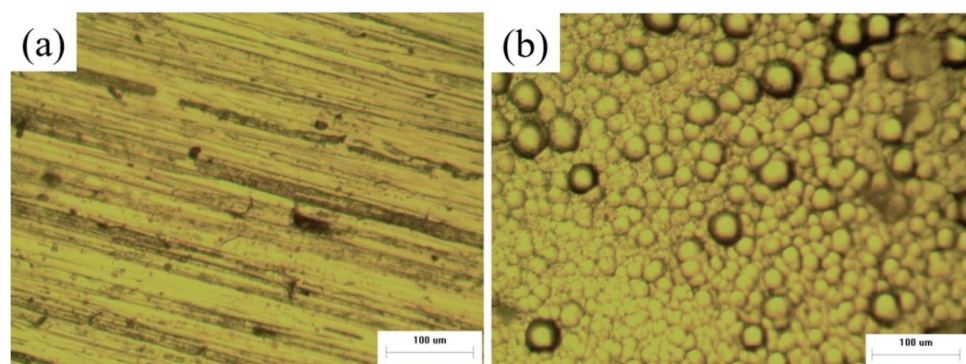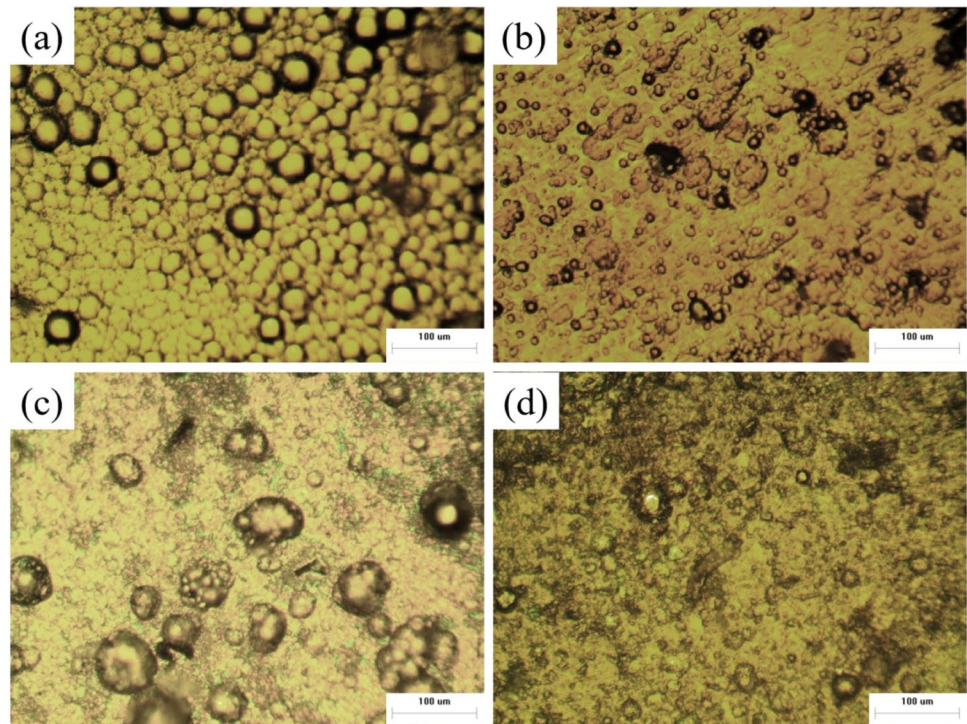
Fig. 9 Surface morphologies of nickel layer at different heat treatment temperatures: **a** without heat treatment, **b** 400 ℃, **c** 500 ℃, **d** 600 ℃

copper and 2.64 kg load are shown in Fig. 6 and Table 3, respectively. The main element of point A is Fe with a small amount of Cr and Cu, indicating that the elements in the brazed filler and 304 stainless steel have diffused to Q235 carbon steel. Point B located on an island consists of Fe, Cr, Ni, and Cu elements, implying that the island is the result of

the diffusion and reaction of the above four elements. Point C consists almost entirely of Cu elements and contains a small amount of Fe, Ni, and Cr elements. The composition of point D located in the 304 stainless steel is close to those of 304 stainless steel base metal.

Fig. 10 Surface morphologies of nickel layer at the different holding times: **a** without heat treatment, **b** 0.5 h, **c** 1 h, **d** 1.5 h
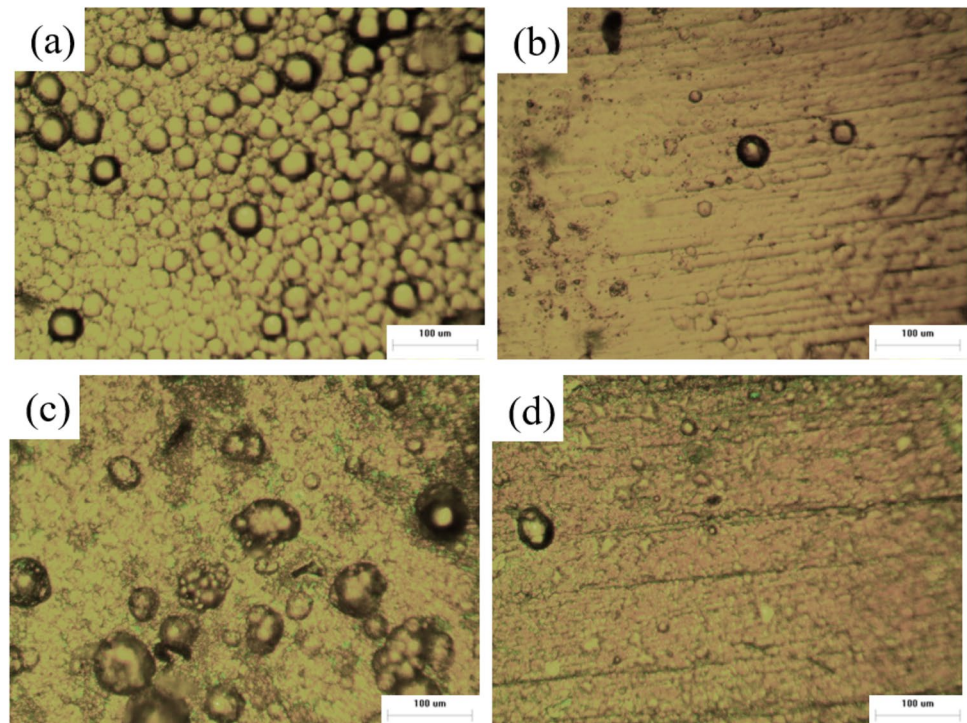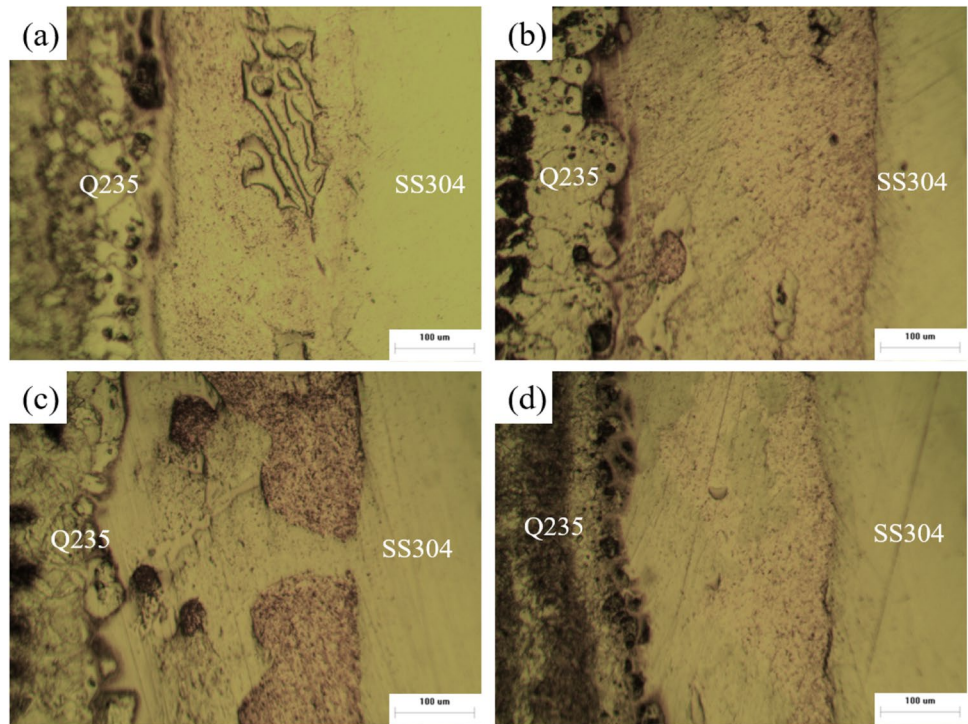
Fig. 11 Metallographic structures of brazed joints after nickel plating at different heat treatment temperatures: **a** without heat treatment, **b** 400 ℃×1 h, **c** 500 ℃×1 h, **d** 600 ℃×1 h

The disparate diffusion rates across distinct locations of the brazed joint result in the formation of a stepped fracture. In Fig. 7a, a large number of parabolic linear toughness nests are elongated along the shear direction, and the width and depth of the toughness nests become smaller and shallower, tending to be flat, and the fracture mode changes from ductile to brittle. In Fig. 7b, a large number of equiaxed tough nests appear, and their width and depth are significantly higher than those in Fig. 7a, when Q235 shows better plastic toughness [28, 29].

Fig. 12 Metallographic structures of brazed joints after nickel plating at different holding times: **a** without heat treatment, **b** 500 ℃×0.5 h, **c** 500 ℃×1 h, (d) 500 ℃×1.5 h
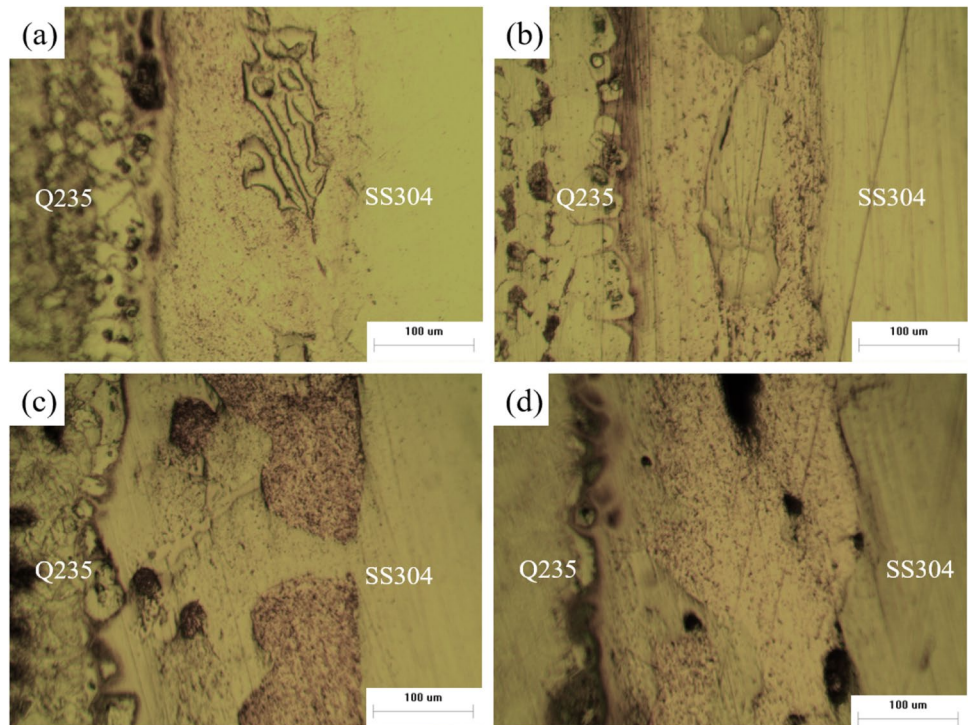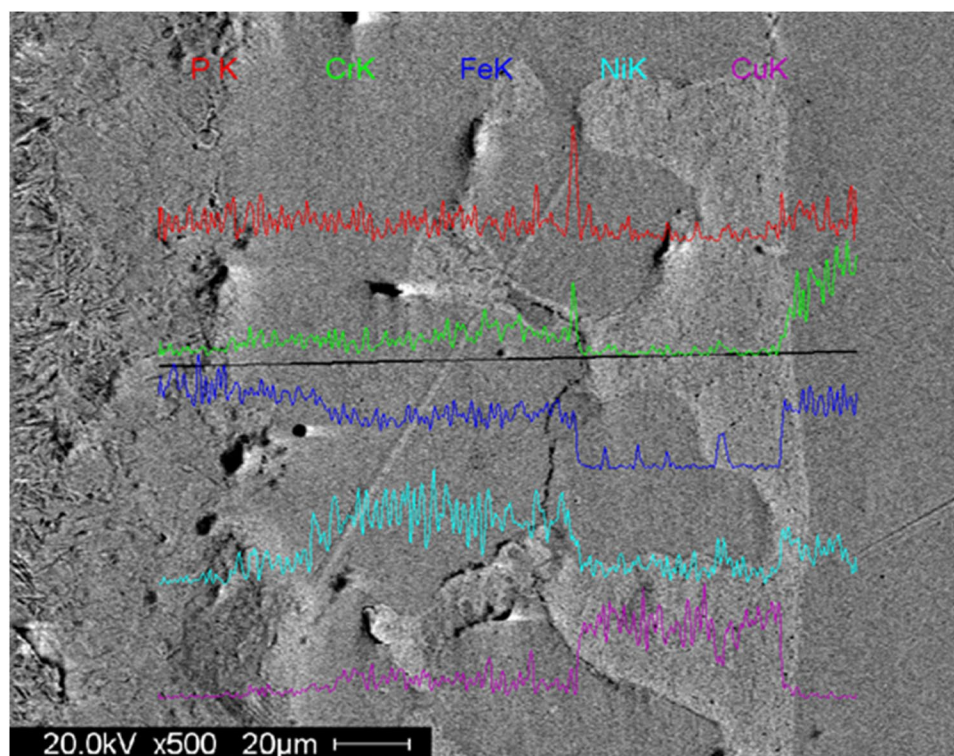
Fig. 13 Element distribution
result of nickel-coated carbon
steel and stainless steel brazed
joint after heat treatment at
500 °C for 1 h

3.2 Microstructure analysis of brazed joint with nickel layer

3.2.1 The surface appearance of a nickel-plated layer

Figure 8 illustrates the alteration of the surface morphology of carbon steel before and after nickel plating, as observed under an optical microscope with a magnification of 400 times. The surface of the carbon steel before nickel plating is characterized by numerous grooves with consistent directionality, which are evidently sandpaper polishing traces. Scattered throughout these grooves are some holes resulting from the grinding process, where gravel was embedded in the metal matrix, and the cleaning process was insufficient to remove them, leaving holes

on the surface. With electroless nickel plating, the surface of the carbon steel is coated with uniformly sized spherical particles that make up the plating structure.

3.2.2 Surface morphology of nickel layer under different heat treatments

Figure 9 shows the surface morphologies of nickel layer at different heat treatment temperatures for 1 h. Before heat treatment, the spherical particles are closely arranged on the surface of the nickel layer and slightly convex with obvious boundaries, as shown in Fig. 9a. After 400 °C heat treatment, the spherical particles of the nickel layer are fused. The boundaries of the particles become blurred and the surface of nickel layer tends to be flat, which is mainly due to the accelerated

Table 4 The shear strength of nickel-coated carbon steel and stainless steel brazed joints

No	Heat-treatment temperature (℃)	Holding time (h)	Shear strength (MPa)	Standard deviation	Coefficient of variation (%)
Without heat treatment	-	-	104.44	7.6	7.3
1	400	1	153.11	12.1	8.0
	500	1	213.37	17.9	8.4
	600	1	137.7	10.4	7.6
2	500	0.5	177.81	12.1	6.8
	500	1	213.37	18.4	8.6
	500	1.5	173.35	11.3	6.5

Fig. 14 The macroscopic appearances of fractures (left: Q235, right: SS304; all section lengths are 15 mm): **a** without heat treatment, **b** 400 ℃×1 h, **c** 500 ℃×0.5 h, **d** 500 ℃×1 h, **e** 500 ℃×1.5 h, **f** 600 ℃×1 h
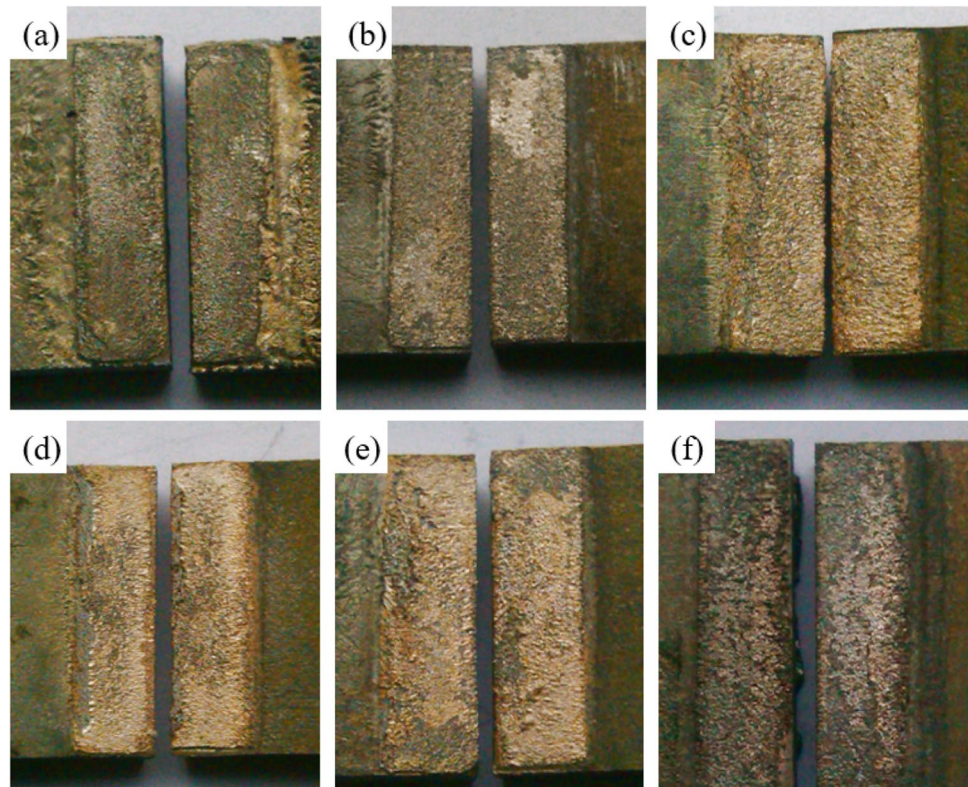
diffusion of atoms caused by the increase in temperature. As the temperature rises to 500 °C, the spherical particles of the nickel layer continue to grow up. In addition, it is difficult to observe the boundaries excluding large spherical particles. It can be seen from Fig. 9d that the spherical particles of the nickel layer after 600 °C heat treatment disappear.

The surface morphologies of the nickel layer after heat treatment at 500 °C for different holding times are shown in Fig. 10. After heat treatment, the spherical particles heated at 500 °C for 0.5 h begin to fuse, showing a strip shape, as shown in Fig. 10b. With increasing holding time to 1 h, the nickel layer shrinks and the surface strip disappears, leaving part spherical particle aggregation and granular precipitates. Finally, a large number of granular precipitates are formed at 500 °C for 1.5 h.

3.2.3 Analysis of bonding interface microstructure in brazed joints

Figure 11 indicates a notable increase in the width of the brazing seam after nickel plating, which is approximately 200 µm, and there are still islands within the brazing seam, albeit in a reduced proportion. The combination interface between the copper brazing material and the stainless steel side appears flat and tight, whereas the combination interface on the nickel-plated carbon steel side appears uneven and possibly defective. The presence

of islands in the brazing seam is more pronounced at higher heat treatment temperatures. This can be attributed to the fact that the islands primarily consist of Fe, and as the heat treatment temperature increases, more Fe diffuses into the brazing seam through the plating, promoting the formation of islands.

Heat treatment at 600 °C results in a broad range of defects at the bonding interface of the plating and copper brazing material, which may be due to the high treatment temperature and the appearance of Ni and P phase precipitates on the surface of the plating [26], leading to the high-temperature formation of intermetallic compounds at the interface between the plating and the brazing material.

The metallographic organization changes observed in Fig. 12 are similar to those shown in Fig. 11. With an increase in the holding time during nickel plating, the Fe content in the nickel layer also increases. During brazing, a large amount of Fe diffuses from the plating to the brazing layer, which promotes the formation of islands in the brazing seam. However, if the holding time is too long, it can result in the formation of excessive plating precipitates, which can lead to the formation of intermetallic compounds at the bonding interface of the brazing material and plating.

Table 5 Materials properties used in FEM calculation [32]

Material	Density (kg/m^3)	Young's modulus (GPa)	Poisson's ratio	Yield stress (MPa)
Q235	7800	210	0.28	235
304	7930	194	0.30	206
Ni	8900	201	0.31	100
Cu	8900	109	0.32	285

3.2.4 Analysis of element diffusion after heat treatment

The element distribution result of nickel-coated carbon steel and stainless steel brazed joint after heat treatment at 500 °C for 1 h is shown in Fig. 13. Ni and P elements in the nickel layer and Fe in carbon steel diffuse into the pure copper intermediate layer. The content of Fe, Cr, and Ni on the island is higher than those of other areas and the content of Cu in the pure copper interlayer is the highest. In addition, P and Cr elements show obvious enrichment at the edge of the island. Gai et al. [30] similarly performed various heat treatments on nickel-based materials to optimize the microstructure and improve the mechanical properties of the wrought superalloy GH4151. The solution treatment mainly affected the γ' precipitate fraction and the γ matrix grain size. A dissolution kinetic model was used to calculate the dissolution of primary γ' precipitates. The results showed that fine primary γ' precipitates dissolved below 1120 °C, while coarse primary γ' precipitates dissolved above 1130 °C.

3.2.5 Fracture morphology and mechanical properties analysis of the joint

Each test uses the least amount of 3 original calculations, average shear strength, and standard deviation. The shear strength of brazed joints with nickel layer is shown in Table 4. The shear strength of the brazed joint after nickel plating at 500 °C for 1 h is 213.37 MPa. However, the shear strength of the unheated brazed joint after nickel plating is only 104.44 MPa. The standard deviation is less than 18, and the minimum standard difference is 7.6 (without heat treatment). The coefficient of variation is less than 9%, and the smallest coefficient of variation is 6.5%, indicating that the dispersion of the experimental results is small.

Figure 14 depicts the fracture morphology of brazed joints under different conditions. It is evident that the fracture of the nickel plating without heat treatment is situated at the nickel plating layer. However, as the heat treatment temperature and holding time increase, the fracture gradually shifts to the copper brazing material layer. This indicates that heat treatment enhances the bonding strength of the nickel plating and carbon steel substrate and can even surpass the shear strength of the copper brazing material. However, if the holding time is too long or the treatment temperature is too high, the fracture occurs at the position where the plating combines with the brazing layer. This indicates that the interaction between the brazing material and the plating is weak. Dinda et al. [31] investigated crystallographic texture changes in electron beam welded dissimilar copper to 304L stainless steel joints using time-of-flight neutron diffraction measurements. It was found that mainly due to the very high thermal conductivity of copper, the main melting occurs on the steel side, while the limiting melting occurs on the copper side. Therefore, a large amount of heat is dissipated from the copper to the steel. Another reason may be due to the limited solid solubility of steel in copper.

In addition, the presence of islands in the weld can also affect the shear strength of the joint. The higher the heat treatment temperature, the more isolated islands are formed due to the diffusion of Fe from the nickel plating layer to the brazing layer, and the thickness of the nickel plating layer becomes thinner, resulting in a decrease in the shear strength
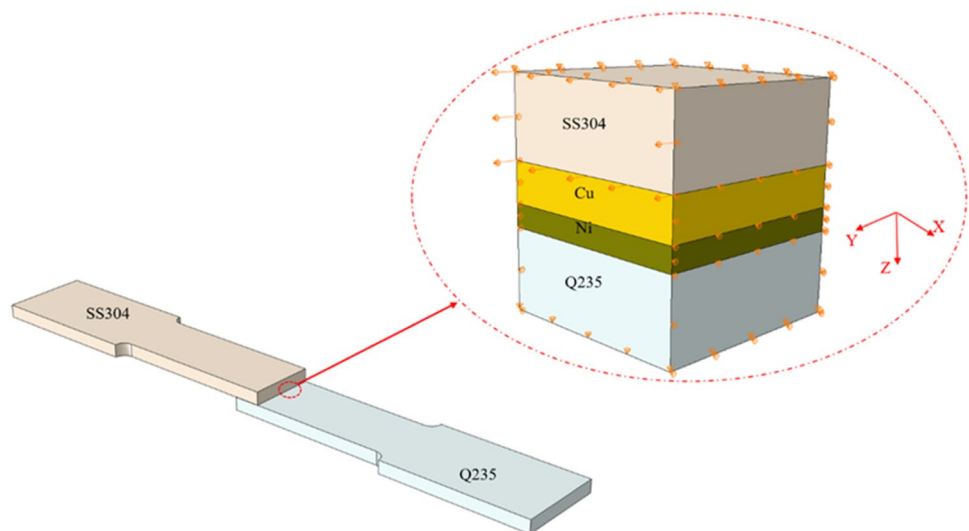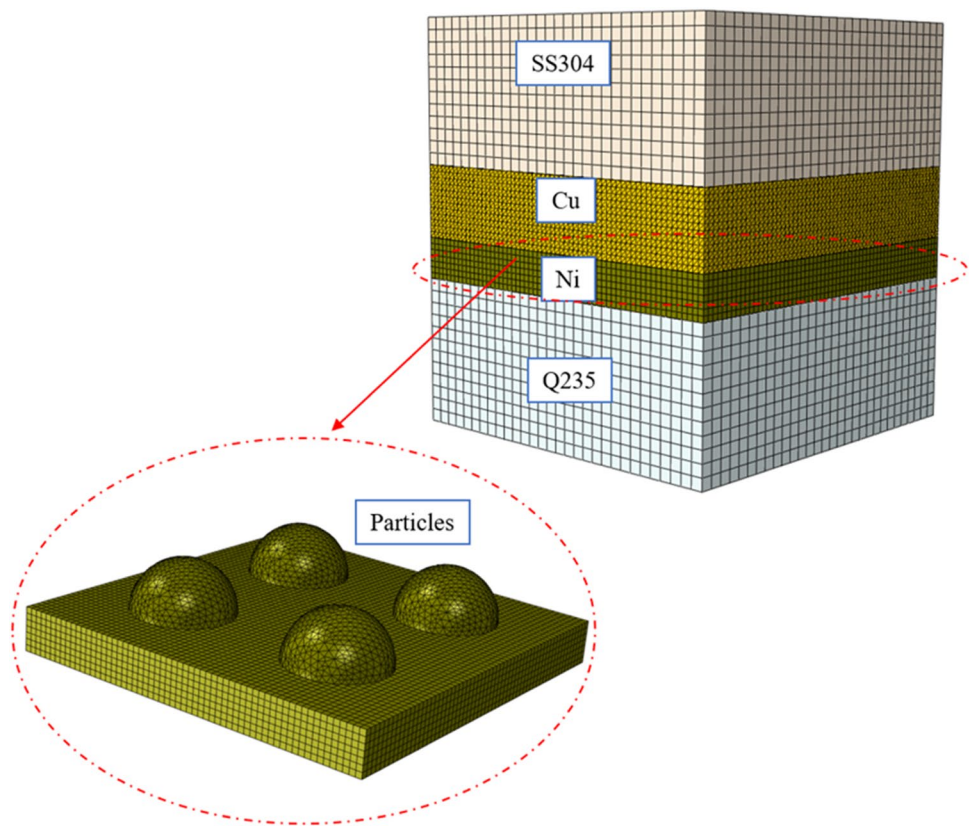
Fig. 15 Sampling location in micro numerical simulation

Fig. 16 Mesh generation

of the joint. The interaction between the brazing material and the nickel layer also plays a crucial role in determining the shear strength of the joint. Although the nickel plating layer becomes thinner after heat treatment, the shear strength tends to decrease, but due to the enhanced interaction between the solder and the nickel plating layer, the shear strength is still higher than that without heat treatment.

4 Finite element model

4.1 Size determination of RVEs

The macro-mechanical responses of the brazed joint are predicted by means of the periodic representative volume element (RVE) technique. The material properties used are listed in Table 5. In the course of the experimental investigation, the emergence of particles on the nickel-plated layer surface was observed. The size of these particles exhibited a trend of initial growth, followed by reduction, as the holding time increased and the holding temperature rose. The most significant particle increase was observed on the plated layer surface after holding at 500 ℃ for 1 h, at which point the brazed joint strength reached its maximum. To elucidate the correlation between particle dimensions and joint strength, a subsequent simulation analysis

was undertaken. The upper plate is made of 304 stainless steel and the lower plate is made of Q235 carbon steel. The material in the middle weld area is pure copper filler metal and a nickel-plated layer.

The initial particle diameter, prior to heat treatment, measured approximately 20 μm. Following a holding period of 1 h, particles at 400 °C exhibited a reduced diameter of approximately 3 μm, while those at 500 °C were the largest, with a diameter of around 50 μm. Particles at 600 °C displayed variable sizes, with the smallest being nearly imperceptible and the largest measuring approximately 20 μm in diameter. In the simulation, spherical particles with diameters of 20 μm, 50 μm, and 80 μm were considered. Composed primarily of Ni, these particles originated from the plating layer, causing a reduction in plating layer thickness as particle size and abundance increased.

The nickel plating, brazing material, and base material were meshed using 10-node tetrahedral elements, while the particles were meshed with 8-node linear hexahedral reduced integral cells. The total mesh count amounted to 297,398, with 46,800 particle meshes and approximately 250,598 remaining meshes. A significant stress concentration was observed at the free edge due to the abrupt change in stiffness, resulting in the initiation of brazing interface peeling at the free boundary. Consequently, the sampling

Fig. 17 Von Mises stress distribution in brazed joints: **a** brazed joint with particles, **b** Von Mises stress distribution along path Z
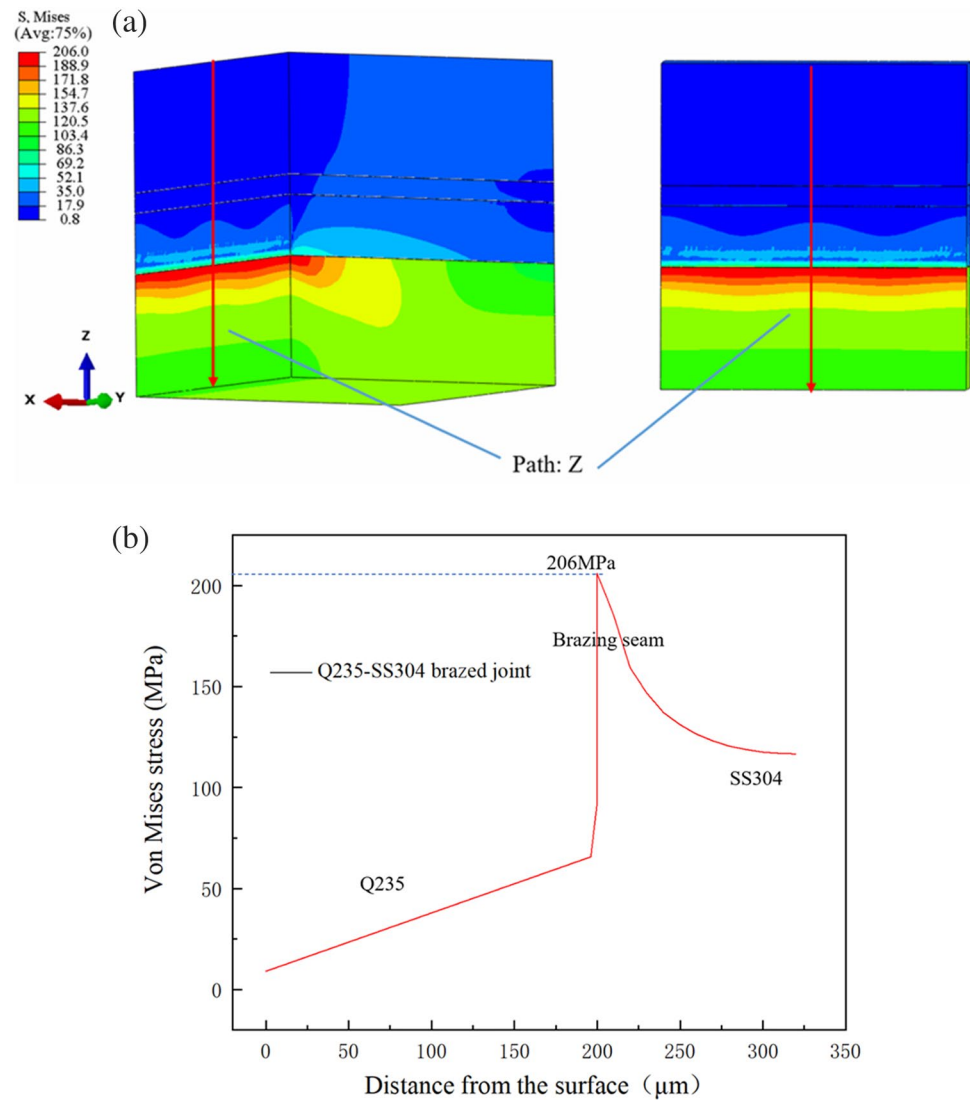
location is depicted in Fig. 15. The mesh generation is shown in Fig. 16.

Owing to the sampling derived from the lap model, disparate materials were mutually constrained during the shearing process. The applied boundary conditions included simple support constraints in the Z and X directions, as well as a specified displacement in the Y-axis direction.

## 4.2 Finite element analysis of shear strength of the brazed joint

The finite element analysis of the shear strength of the brazed joints was carried out using ABAQUS finite element software in the mm unit system.

Figure 17 shows the equivalent force clouds of Q235-Ni, Ni-Cu, and Cu-SS304 brazed joints. The center

point of the upper and lower edges of the base material on both sides of the symmetry plane is taken as the starting point for path Z, and the equivalent force distribution along path Z is shown in Fig. 17b. From Fig. 17a, it can be seen that the Mises stresses in the brazed joint are mainly concentrated in the brazing area and the edges of the brazing surface of the SS304 base material. On the brazing surface of SS304, the maximum residual stress appears on the copper brazing material side, which is 206 MPa. The stress on the Q235 base material side containing the nickel plating layer is smaller, and the stress from the Q235 base material to SS304 is distributed in a peak-like pattern, with the maximum stress at the weld seam.

In order to further analyze the distribution of residual stress at special locations in the joint, path X is selected in the brazing seam area.

Fig. 18 **a** Path diagram, **b** Von Mises stress distribution along path X
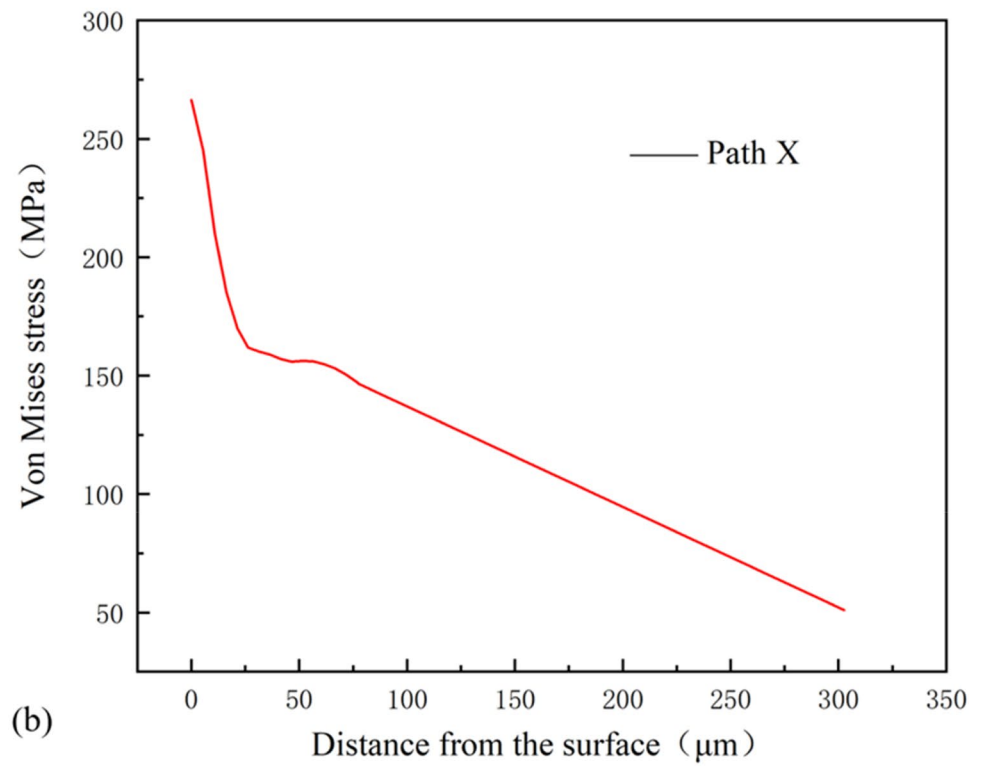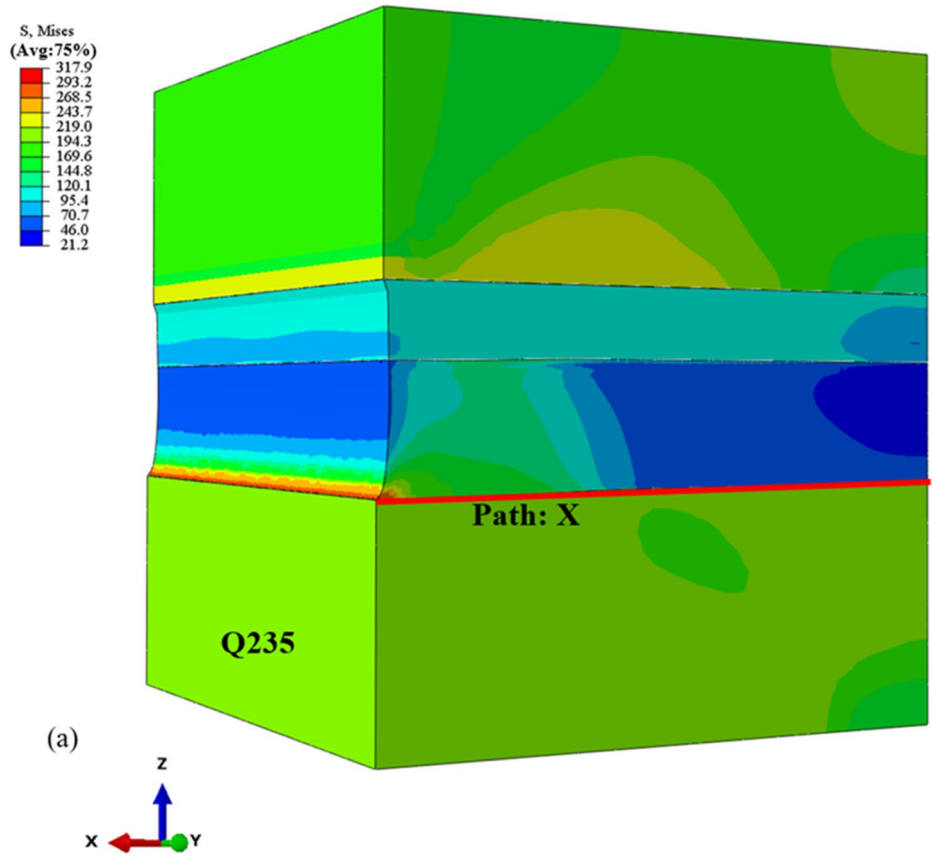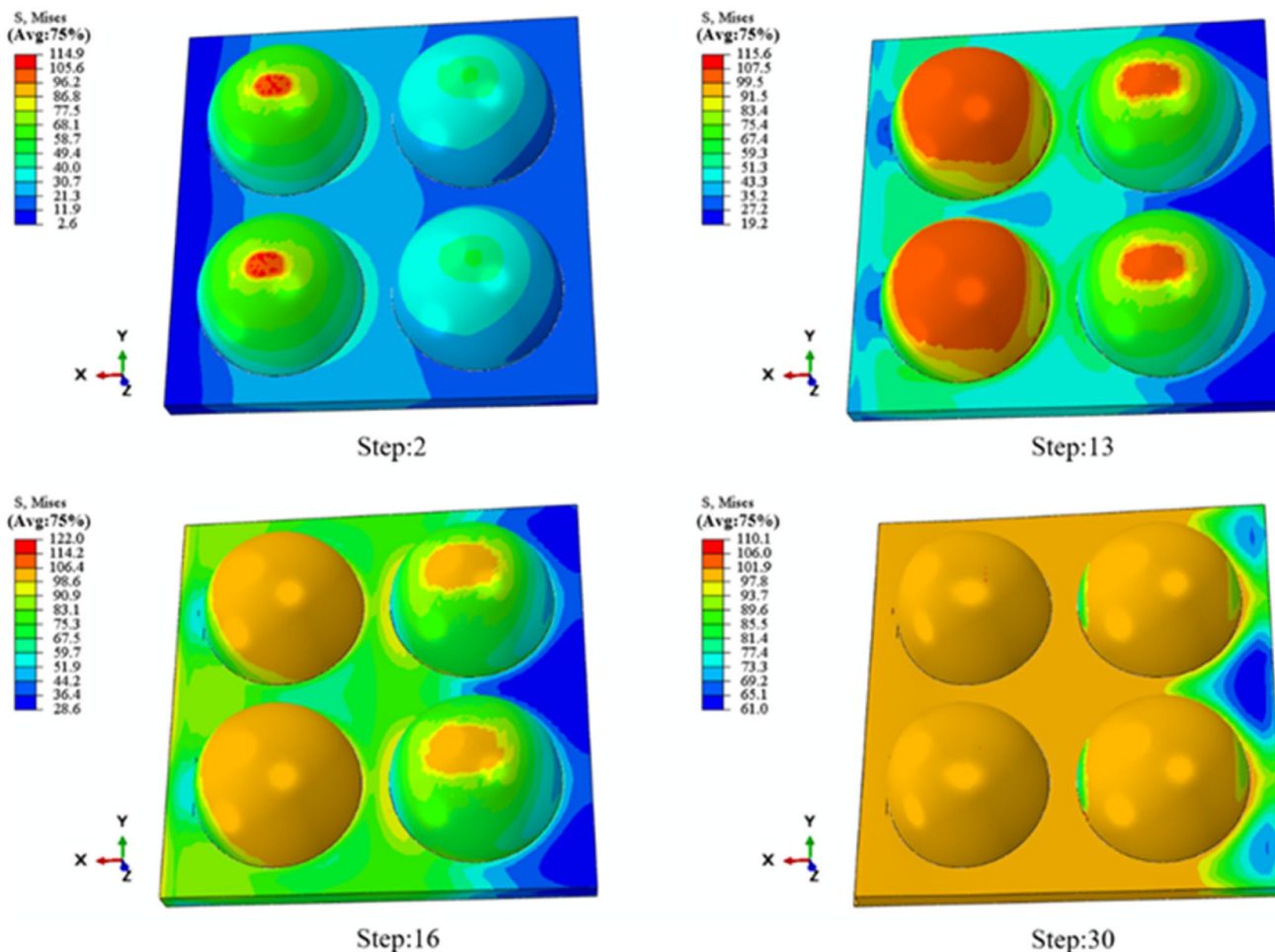
Fig. 19 Mises stress distribution of particles and nickel-plated layer at different times

As is shown in Fig. 18, in the X-axis direction, the Mises stress generally presents a downward trend, and the closer it is to the loading surface, the faster the stress decreases. Due to its ideal elastic model, under uniform loading, the stress decreases linearly after 75 µm.

Figure 19 presents a comparison of the stress changes between the nickel-plated layer and the particles at different stages. The observation from the figure suggests that the stress gradually transfers from the center of the particles to the plating, and the stress level of the particles remains higher than that of the plating. This implies that the particles have a stress-dispersing effect during the process.

Figure 20 displays the stress–strain curves for various nickel particle sizes and plating thicknesses. The brazed joints with 120-µm nickel particles achieve the highest shear strength of 187.4 MPa, while the maximum strength for a particle diameter of 50 µm is greater than that for 80 µm. The highest shear strength of 213.4 MPa is obtained at a heat treatment temperature of 500 °C and a holding time of 1 h for both particle sizes.

Figure 21 illustrates the stress–strain curves for different nickel plating thicknesses. The results indicate that plating nickel to improve corrosion resistance decreases the shear strength, and the optimal plating thickness after nickel plating is 20 µm, which is in line with the experimental findings. The simulation results show that the higher shear strength after brazing is achieved when the particle diameter is 50 µm and the plating thickness is 20 µm, consistent with the experimental results.

According to the experimental findings, it is observed that increasing the heat treatment temperature leads to a higher number of islands in the brazing seam. This is attributed to the fact that the islands mainly contain Fe, and the higher diffusion of Fe from the plating to the seam occurs at higher temperatures. This facilitates the formation of islands in the seam. At a heat treatment temperature of 600 °C, a wide range of defects is observed at the bonding interface of the plating and copper brazing material. This can be attributed to the formation of Ni and P phase precipitates on the surface of the plating and the

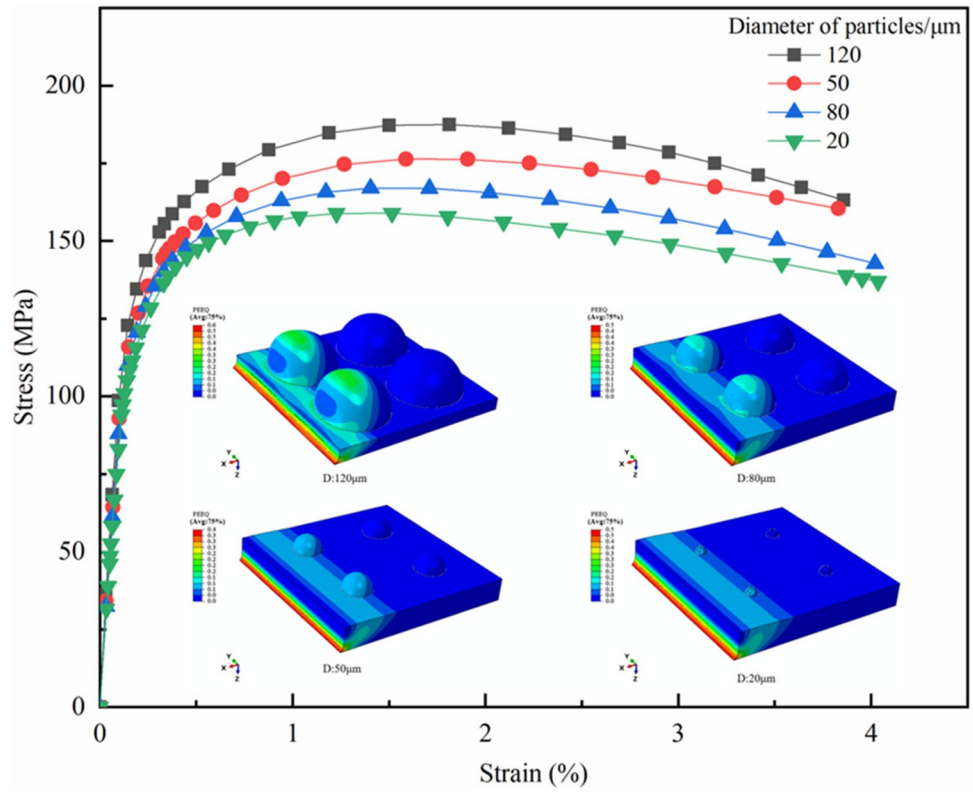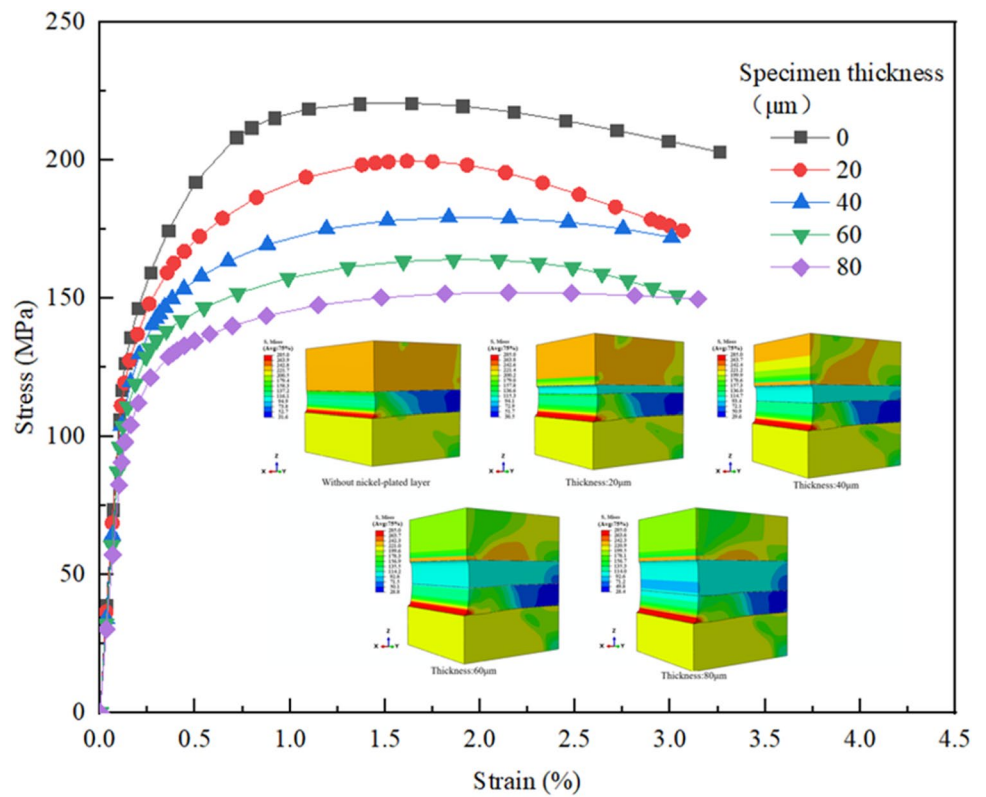**Fig. 20** Stress–strain curves of different nickel particle sizes

Fig. 21 Stress–strain curves of different nickel plating thicknesses

formation of high-temperature intermetallic compounds at the interface of the plating and brazing material due to the high heat treatment temperature.

5 Conclusions

This paper investigates the shear strength, microstructure, and element distribution of brazed joints between Q235 steel and 304 stainless steel structural parts using pure copper as the brazing material and vacuum brazing technique. The effect of the thickness of the brazing material on the quality of the brazed joints was explored, and the properties related to the welded joints were compared with those of carbon steel plated with nickel, and heat treated after nickel plating. ABAQUS finite element analysis software was used to simulate the effect of nickel plating layer thickness and spherical particle size on the joint strength. The main findings and conclusions of this paper are summarized as follows:

A) The pure copper brazing material exhibited good wettability to the two base materials at high temperatures, resulting in sufficient caulking and dense bonding of the brazing material and base material without defects. The shear strength of the welded joint with 0.06-mm brazing material was found to be the highest, reaching 265.9 MPa.

B) During the brazing process, islands are produced at the Q235 steel/copper interface and extend vertically from the brazing seam to the stainless steel side, produced from copper, containing Fe, Cr, Ni, and Cu elements in an iron-rich phase. When the brazing seam width is small, the islands can cross the brazing seam and connect the carbon steel and stainless steel. When the brazing seam width is large, the islands extend from the Q235 steel/304 stainless steel interface toward the brazing layer, with some islands being separated from the interface and free in the brazing seam in the form of isolated islands.

C) Ni plating was prepared on the surface of Q235 carbon steel by a chemical plating method, with a uniform thickness of about 20 μm. The nickel-plated samples were then subjected to heat treatment at different temperatures and holding times. With the increase of heat treatment temperature and holding time, the particles of the plating fused; the boundary of the particles gradually disappeared; the diffusion distance of Fe, Ni, and P elements increased; the interface transition zone became wider; and granular precipitates appeared on the surface of the plating.

D) The shear strength of brazed joints after nickel plating was 213.4 MPa at 500 °C for 1 h, while the shear strength of brazed joints after nickel plating without heat treatment was only 104.4 MPa. Compared to brazed samples without nickel plating, the shear strength of brazed joints of carbon steel after nickel plating was reduced. Additionally, the higher the heat treatment temperature after nickel plating, the more islands were present in the brazed joints.

E) The simulation results show that the shear strength after brazing is higher when the particle diameter is 50 μm and the plating thickness is 20 μm, which is consistent with the experimental results. The damaged region was located at the interface of Cu/stainless steel and nickel plating/Q235.

Author contribution Leilei Wang: methodology, investigation, software, visualization, data curation, writing—original draft, writing—review and editing.

Nian Li: conceptualization, resources, writing-review and editing, project administration, supervision.

Xinlong Wei: formal analysis, writing—review and editing, supervision.

Xiang Ling: writing—review and editing, funding acquisition, resources, supervision.

Qingsheng Li: Writing—review and editing, supervision.

Data Availability The data that support the findings of this study are available from the corresponding author, [Li Nian], upon reasonable request.

Declarations

Competing interests The authors declare no competing interests.

References

1. Hu D, Li Y, Liu P et al (2022) Numerical study on the effect of nozzle incident angle on the overall performance of gas wave refrigerator [J]. Int J Refrig 138:61–70

2. Li RF, Yu ZS, Qi K (2013) Vacuum brazing of GH2132 superalloy using BNi-2+BNi-5 composite filler [J]. Adv Mater Res 2108(1206):2087–2091

3. Li Y, Chen C, Yi R et al (2020) Special brazing and soldering [J]. J Manuf Process 60:608–635

4. Way M, Willingham J, Goodall R (2020) Brazing filler metals [J]. Int Mater Rev 65(5):257–285

5. Ojo OA, Richards NL, Charturvedi MC (2004) Effect of gap size and process parameters on diffusion brazing of Inconel 738 [J]. Sci Technol Weld Join 9(3):209–220

6. Tetsui T (2001) Effects of brazing filler on properties of brazed joints between TiAl and metallic materials [J]. Intermetallics 9(3):253–260

7. Ahn B (2021) Recent advances in brazing fillers for joining of dissimilar materials [J]. Metals 11(7):1037

8. Luo Q, Xue S, Wu J (2021) Influences of Sn on properties of Ag-based and Cu-based brazing filler metals [J]. Crystals 11(11):1403

9. Hissyam W, Aiman MH, Ishak M et al (2019) Effect of copper based filler composition on the strength of brazed joint [J]. J Mech Eng Sci 13(2):5090–5103

10. Beura VK, Xavier V, Venkateswaran T et al (2018) Interdiffusion and microstructure evolution during brazing of austenitic martensitic stainless steel and aluminum-bronze with Ag-Cu-Zn based brazing filler material [J]. J Alloy Compd 740:852–862

11. Li Y, Parfitt D, Flewitt PEJ et al (2020) Microstructural considerations of enhanced tensile strength and mechanical constraint in a copper/stainless steel brazed joint [J]. Mater Sci Eng A 796:139992

12. Mai TA, Spowage AC (2004) Characterisation of dissimilar joints in laser welding of steel–kovar, copper–steel and copper–aluminium [J]. Mater Sci Eng A 374(1–2):224–233

13. Wang XG, Yan FJ, Li XG et al (2017) Induction diffusion brazing of copper to aluminium [J]. Sci Technol Weld Join 22(2):170–175

14. Xiao Y, Ji H, Li M et al (2013) Ultrasound-assisted brazing of Cu/Al dissimilar metals using a Zn–3Al filler metal [J]. Mater Des (1980-2015) 52:740–747

15. Cai ZP, Ai BQ, Cao R et al (2016) Microstructure and properties of aluminum AA6061-T6 to copper (Cu)-T2 joints by cold metal transfer joining technology [J]. J Mater Res 31(18):2876–2887

16. Jiang YU, Xinglin M, Zhang H et al (2023) Feasibility study of thermo-compensated resistance brazing welding of C/C composites and T2 copper with AgCuTi filler metal [J]. Chin J Aeronaut 36(5):534–548

17. Solchenbach T, Plapper P (2013) Mechanical characteristics of laser braze-welded aluminium–copper connections [J]. Opt Laser Technol 54:249–256

18. Zhao B, Zhou H, Ding Y et al (2022) Wavy microstructure for improvement of bonding strength in titanium to carbon steel brazed joints [J]. J Mater Process Technol 305:117572

19. Choudhary RK, Laik A, Mishra P (2017) Microstructure evolution during stainless steel-copper vacuum brazing with a Ag/Cu/Pd filler alloy: effect of nickel plating [J]. J Mater Eng Perform 26:1085–1100

20. Mu G, Qu W, Zhang Y et al (2023) Effect of Ni on the wetting and brazing characterization of 304 stainless steel by Ag–Cu alloy [J]. J Mater Sci 58(14):6297–6312

21. Zhang WW, Cong S, Huang Y et al (2017) Micro structure and mechanical properties of vacuum brazed martensitic stainless steel/tin bronze by Ag-based alloy [J]. J Mater Process Technol 248:64–71

22. Zhang C, Wu M, Pu J et al (2023) Effect of Ni coating on microstructure and property of Al alloy/steel CMT welding-brazing joints [J]. Coatings 13(2):418

23. Kumar A, Ganesh P, Kaul R et al (2016) Study on requirement of nickel electroplating in OFE copper-316L stainless steel brazed joints [J]. Int J Adv Manuf Technol 87:2639–2651

24. Sanchez L, Carrillo D, Rodriguez E et al (2011) Development of high precision joints in particle accelerator components performed by vacuum brazing [J]. J Mater Process Technol 211(8):1379–1385

25. Mu G, Qu W, Zhang Y et al (2023) Effect of Ni on grain boundary penetration in vacuum brazing of copper and stainless steel [J]. Weld World 67(2):483–494

26. Ashassi-Sorkhabi H, Rafizadeh SH (2004) Effect of coating time and heat treatment on structures and corrosion characteristics of electroless Ni–P alloy deposits [J]. Surf Coat Technol 176(3):318–326

27. De Prado J, Sánchez M, Ruiz A et al (2020) Effect of brazing temperature, filler thickness and post brazing heat treatment on the microstructure and mechanical properties of W-Eurofer joints brazed with Cu interlayers [J]. J Nucl Mater 533:152117

28. Liu J, Shukui L, Xiaoqing Z et al (2008) Adiabatic shear banding in a tungsten heavy alloy processed by hot-hydrostatic extrusion and hot torsion[J]. Scripta Materialia 59(12):1271–1274

29. Su YS, Li SX, Yu F et al (2021) Revealing the shear band origin of white etching area in rolling contact fatigue of bearing steel [J]. Int J Fatigue 142:105929

30. Gai Y, Zhang R, Yang J et al (2022) Effects of heat treatment on γ′ precipitates and tensile properties of a Ni-base superalloy [J]. Mater Sci Eng, A 842:143079

31. Dinda SK, Kar J, Roy GG et al (2020) Texture mapping in electron beam welded dissimilar copper-stainless steel joints by neutron diffraction [J]. Vacuum 181:109668

32. Arenas MF, Acoff VL, Reddy RG (2004) Physical properties of selected brazing filler metals [J]. Sci Technol Weld Join 9(5):423–429